# Wavelet-based analysis of enstrophy transfers in two-dimensional turbulence

- 3 Patrick Fischer and Charles-Henri Bruneau
- 4 IMB Université Bordeaux 1, INRIA Team MC<sup>2</sup>, CNRS UMR 5251, 351, cours de la Libération,
- 5 33405 Talence, France
- 6 (Received 7 November 2008; accepted 11 May 2009; published online xx xx xxxx)
- 7 Two-dimensional turbulence admits two different ranges of scales: a direct enstrophy cascade from
- 8 the injection scale to the small scales and an inverse energy cascade at large scales. It has already
- 9 been shown in previous papers that vortical structures are responsible for the transfers of energy
- upscale while filamentary structures are responsible for the forward transfer of the enstrophy. Here
- we propose an original mathematical tool, the interaction function, for studying the space
- 12 localization of the enstrophy fluxes. It is defined using an orthogonal two-dimensional wavelet
- decomposition. © 2009 American Institute of Physics. [DOI: 10.1063/1.3153910]

#### 15 I. INTRODUCTION

Two-dimensional turbulence has interested and contin-17 ues to interest different scientific communities. Its relevance 18 to atmospheric and oceanic flows at large scales has largely 19 motivated its detailed study. 1-3 Its importance for the under-20 standing of turbulence, in general, due to the existence of 21 two cascades, as opposed to the direct cascade of energy in 22 three dimensional turbulence, is another reason to study this 23 phenomenon. While three dimensional turbulence is gov-24 erned by a direct cascade of energy from the scale of injec-25 tion to the small scales where the energy is dissipated, two-26 dimensional turbulence admits two different ranges.<sup>4,5</sup> The 27 first one is governed by an inverse energy cascade from the 28 scale of injection to the large scales. The second one is gov-29 erned by a cascade of enstrophy from the scale of injection to 30 the small scales. This scenario, proposed by Kraichnan and 31 Batchelor over 40 years ago, finds confirmation in many dif-**32** ferent numerical simulations and experimental realizations 33 (see, for example, Refs. 6–11). According to the Kraichnan 34 theory, at large scales, the energy spectrum has the form **35**  $E(k) \propto k^{-5/3}$  while at small scales it is  $E(k) \propto k^{-3}$ . However, **36** for the direct cascade at small scales,  $^{12-17}$  found spectra **37** steeper than  $k^{-3}$  in earlier simulations and experiments. We 38 also observed steeper energy spectra in our particular two-**39** dimensional set up 18-20 confirming these earlier results.

Two distinct kinds of structures can be detected in two-41 dimensional turbulent flows: vortical structures and filamen-42 tary structures. The first play an important role for the in-43 verse transfers of energy while the filamentary structures can 44 be associated with the forward transfers of enstrophy. These 45 links between the presence of structures and the transfer of 46 energy or enstrophy have been observed by many authors as 47 Refs. 17 and 19–23.

The inverse energy cascade, whose the merging of same 49 sign vortices is probably one of the mechanisms, transfers 50 energy from the injection scale to the large scales. At scales 51 smaller than the injection scale, an enstrophy cascade, whose 52 origin is certainly the straining of vorticity gradients, trans-53 fers enstrophy from large to small scales. The wavelet de-54 compositions used for filtering the turbulent flows have been

introduced and extensively studied by Farge and Rabreau 55 since 1988 (Refs. 24 and 25; see also her webpage for an 56 exhaustive list of publications: http://wavelets.ens.fr). How- 57 ever, the usual wavelet-based methods do not allow us to get 58 a precise space localization of the enstrophy fluxes. We 59 know, according to the classical theory and to numerous nu- 60 merical simulations, that the enstrophy transfers are small- 61 scale physical transfers. We also know that the filamentary 62 structures are responsible for these transfers. However, we 63 do not know yet if these transfers uniformly occur every- 64 where in the flow and if not, where these transfers precisely 65 take place. Very recent work points out that the mechanism 66 behind these two cascades is the thinning of vortices. 21,22 67 Stretching of small-scale vorticity gradient by the strain aris- 68 ing from larger-scale vortices is believed to be the mecha- 69 nism for the enstrophy cascade. Thus the forward enstrophy 70 flux should mainly occur in strain-dominated regions of the 71 flow. Using a Gaussian-based filtering and the Weiss 72 criterion, <sup>26</sup> Ref. 21 showed that the enstrophy flux is either 73 forward or backward with almost equal likelihood in vortic- 74 ity regions, but tends to be mainly forward in the strain re-75 gions. However, this scale Gaussian-based filtering is unable 76 to accurately detect the very spatially localized events re-77 sponsible for the enstrophy cascade. Quoting, <sup>17</sup> "Local fluxes 78 are strongly inhomogeneous in physical space: there are 79 relatively small regions of intense (positive and negative) flux 80 in both the energy and enstrophy inertial ranges," we pro- 81 pose here a complementary mathematical tool for the analy- 82 sis of the enstrophy flux. We call this mathematical object the 83 interaction function since it describes the interactions respon- 84 sible for the enstrophy transfers in the flow. It is based on 85 two-dimensional orthogonal wavelet decompositions of the 86 two terms involved in the transport term of the Navier-87 Stokes equations.

#### II. THE INTERACTION FUNCTION

The motion of an incompressible viscous fluid in a two- 90 dimensional channel may be described by the vorticity equa- 91 tion obtained by taking the curl of the Navier–Stokes equa- 92 tion: 93

$$\frac{\partial \omega}{\partial t} + (\boldsymbol{v} \cdot \boldsymbol{\nabla})\omega = \frac{1}{\text{Re}} \nabla^2 \omega + f. \tag{1}$$

1-2

95 The velocity field is denoted by  $\mathbf{v} = (u, v, 0)$  and the vorticity **96** by  $\omega = \nabla \times v = (0, 0, \omega)$  with  $\omega = (\partial v / \partial x) - (\partial u / \partial y)$ . In Eq. (1), 97  $(\boldsymbol{v} \cdot \nabla) \omega$  is the transport term,  $(1/\text{Re})\nabla^2 \omega$  the dissipation 98 term due to the viscosity and f a potential forcing term. In 99 the computations presented in the sequel, the forcing term is 100 taken equal to zero and the turbulence is naturally created by 101 obstacles in a channel.

102 The enstrophy flux derives from the nonlinear transport 103 term in the vorticity equation written in Fourier space

$$\Pi_Z(k) = \int_k^{+\infty} T_Z(k') dk', \qquad (2)$$

**105** where the enstrophy transfer function  $T_z(k)$  is obtained by **106** angular integration of  $N_Z(\omega) = \omega^*(k) \cdot (\mathbf{v} \cdot \nabla) \omega(k)$ .

We can replace the Fourier transform by a wavelet trans-108 form leading to a different representation of the enstrophy 109 transfers in the flow. The method we propose here leads to an 110 original representation, called the enstrophy interaction func-111 tion. The term  $N_Z(\omega)$  is, in fact, a scalar product, in Fourier 112 space, between the vorticity field  $\omega$  and its transported field 113  $(\boldsymbol{v} \cdot \nabla)w$ . If the transported field is spectrally close to the 114 initial vorticity field then  $N_Z(\omega)$  will be large but if it is very 115 different or even orthogonal then  $N_Z(\omega)$  will be insignificant. 116 So, the term  $N_Z(\omega)$  measures the correlation, in Fourier 117 space, between the transported and the initial vorticity fields. 118 This correlation is then used to compute the transfer function 119  $T_Z$  and the enstrophy flux  $\Pi_Z$ . By using a Fourier transform, 120 we obtain a description of the enstrophy transfers through the **121** scales, but all the information about the space localization of 122 these transfers is completely lost. However, it is well known, 123 from the classical theory of two-dimensional turbulence and 124 from numerical experiments, that the direct enstrophy cas-125 cade takes place from the injection scale to the smallest 126 scales. The enstrophy cascade is thus essentially a small 127 scales phenomenon and may be localized in space. The 128 method we propose in this paper is based on a two-129 dimensional wavelet transform and leads to a space-scale 130 description of the enstrophy transfers. It consists in replacing 131 the usual Fourier transform in the computation of  $N_Z(\omega)$  by a 132 wavelet transform. The interaction function for the enstrophy 133 transfer is obtained through a three step process:

- **134** (1) Computation of the two-dimensional orthogonal wavelet transforms of  $\omega(k)$  and  $(\boldsymbol{v} \cdot \nabla)\omega(k)$ . This step leads to the 135 136 space-scale representations of these two terms. The re-137 sults of these transforms are denoted by  $WT(\omega)$  and  $WT((\boldsymbol{v} \cdot \nabla)\omega)$  in the sequel. 138
- 139 (2) Computation of the scalar product of  $WT(\omega)$  and  $WT((\boldsymbol{v}\cdot\boldsymbol{\nabla})\omega)$ . The result of this product is a wavelet-140 based representation of the interactions responsible for 141 the enstrophy transfers. The coefficients obtained here 142 will be strong if the strong coefficients of  $WT(\omega)$  and 143  $WT((\boldsymbol{v}\cdot\nabla)\omega)$  are localized at the same place and the 144 same scale. In the usual enstrophy flux computation in 145 Fourier space, the space information is completely lost 146 147 and only scale localizations are considered.

(3) Reconstruction in the physical space, using an inverse wavelet transform, of the result obtained at the previous 149 step. This last step restitutes in physical space the inter- 150 actions between WT( $\omega$ ) and WT(( $\boldsymbol{v} \cdot \nabla$ ) $\omega$ ) occurring at 151 various scales. The result of this last computational step 152 is by definition the interaction function and is denoted 153 by IF<sub>7</sub>.

This three steps algorithm can be summarized by the 155 formula

$$IF_{Z} = WT^{-1}[WT(\omega)WT((\boldsymbol{v} \cdot \nabla)\omega)], \tag{3}$$

where WT denotes the two-dimensional wavelet transform 158 and WT<sup>-1</sup> its inverse transform. The interaction function is 159 used by itself, but is not used to compute the enstrophy flux 160 which does not give any spatial information. It can be con- 161 veniently represented onto a contour plot of the vorticity 162 field. No thresholding is applied on the wavelet coefficients, 163 but the color representation enhances the regions correspond- 164 ing to strong enstrophy interactions. So the wavelet trans- 165 form gives a space-scale representation of the object under 166 study. When performing the scalar product, we compare, in 167 fact, the wavelet decompositions of the two terms involved 168 in the product. If the two terms have the same behavior at the 169 same place and the same scale then the result of the scalar 170 product will present large coefficients at the corresponding 171 scale and place. Then by applying an inverse wavelet trans- 172 form we can get a space representation of the interactions 173 involved in the enstrophy transfers. The same process can be 174 used for the energy transfers using the corresponding data. 175

# **III. NUMERICAL TESTS ON TWO TEXTBOOK CASES**

176

177

200

A first textbook case of the interaction function is given 178 in Fig. 1. This figure corresponds to the simulation of the 179 evolution of two vortices of different signs in a  $2\pi$  periodic 180 square domain. After a while a third but less energetic vortex 181 is created. The interaction function mainly focus on the two 182 original vortices where the strong interactions take place. A 183 second textbook case is presented in Figs. 2 and 3. In this 184 experiment, 14 vortices of different signs have been ran- 185 domly dispatched in a  $2\pi$  periodic square domain. During 186 the decaying process, some vortices merged and we obtained 187 the vorticity field shown in Fig. 2. As can be easily noticed, 188 the interaction function points to one particular event. Com- 189 puting the enstrophy fluxes corresponding to the whole flow 190 and to a small area delimited by the interaction function 191 allows us to show that the interaction function effectively 192 points to the main event in the flow (Fig. 3).

The relevance and the interest of the interaction function 194 cannot be fully assessed on mere examples like those pre- 195 sented here since they correspond to decaying homogeneous 196 isotropic turbulent flows and thus the notion of enstrophy 197 cascade is limited. The power of this new mathematical func- 198 tion is presented in the next part where fully developed tur- 199 bulence simulations are carefully analyzed.

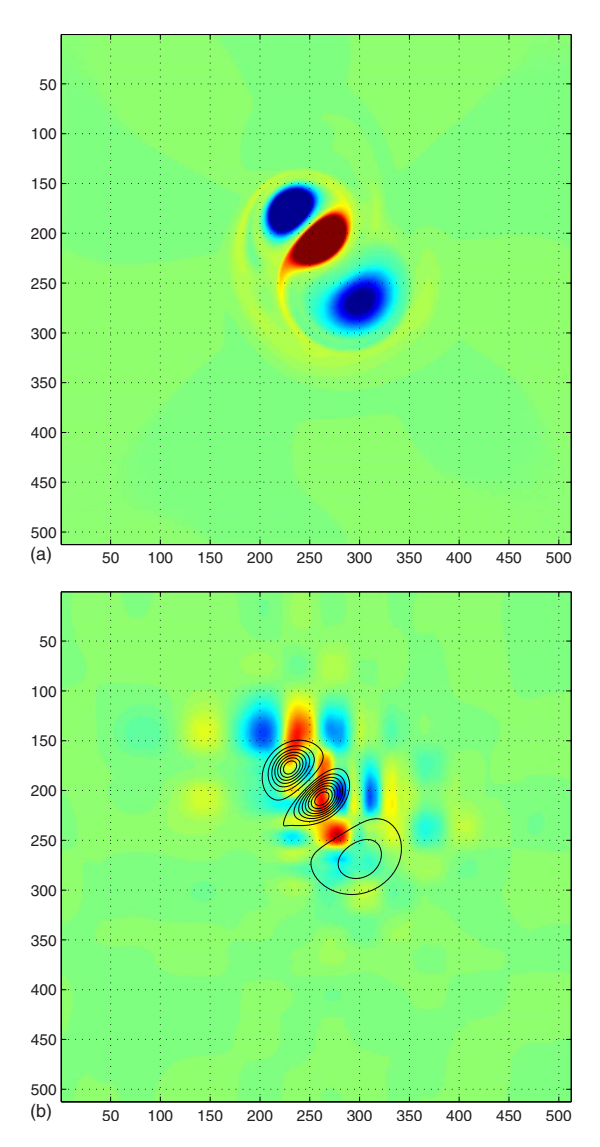


FIG. 1. (Color online) Two vortices interacting and giving birth to a third one. (a) Vorticity field. (b) Interaction function with contour lines of vorticity.

IV. EXPERIMENTAL SETUP

# 500 (b) 100 200 300 400 FIG. 2. (Color online) Fourteen vortices of different signs interacting in a contour lines of vorticity. studied with classical periodic domain conditions and requires particular set up as we study here. Indeed, the numeri- 221 cal setup and the interaction function method presented here 222 are particularly well adapted for studying boundary vorticity 223 creation.

202 The numerical experiments presented in this paper have 203 been originally motivated by experiments carried out with 204 soap films where grid turbulence was studied in details. 13,27 205 They consist in the numerical simulation of a two-206 dimensional channel flow perturbed by an horizontal array of 207 cylinders. Two vertical arrays of additional cylinders have 208 been added in order to increase the number of vortices, and 209 thus to enhance the turbulent behavior of the flow. <sup>18</sup> The 210 numerical results obtained through such direct numerical 211 simulation are the same than those discussed in Ref. 18. 212 They can be compared to those obtained by soap film experi-213 ments where the flow is perturbed by analogous arrays of 214 small cylinders. 18

This unusual set up is more related to realistic cases than 216 the classical two-dimensional periodic domain approach. It 217 corresponds to a river flowing under a bridge with the cylin-218 ders playing the role of the bridge pillars. Furthermore, the 219 production of vorticity by real physical boundaries cannot be

 $2\pi$  periodic domain. (a) Whole vorticity field. (b) Interaction function with

The length of the rectangular channel  $\Omega$  is four times its 225 width L and the Reynolds number based on the cylinders 226 diameter is Re=5000. In this experiment, the cylinders create 227 and maintain the turbulent behavior of the flow. Thus the 228

injection scale  $k_{\rm inj}$  is given by the diameter of cylinders L/8 229 and consequently the injection scale is around  $k_{\text{ini}}$ =8. We use 230 here a large injection scale as we focus on the enstrophy 231 cascade range (Fig. 4).

The penalization method is used to solve the flow around 233 the obstacles. Consequently the Brinkman-Navier-Stokes 234 equations are solved in the whole channel  $\Omega$  including the 235

solid obstacles  $\Omega_s$  and the fluid domain  $\Omega_f$ . This problem has 236 been theoretically studied in Ref. 28. The equations are discretized in time by a second-order 238 Gear scheme with an implicit treatment of the linear terms 239

224

1-4 P. Fischer and C.-H. Bruneau Phys. Fluids 21, 1 (2009)

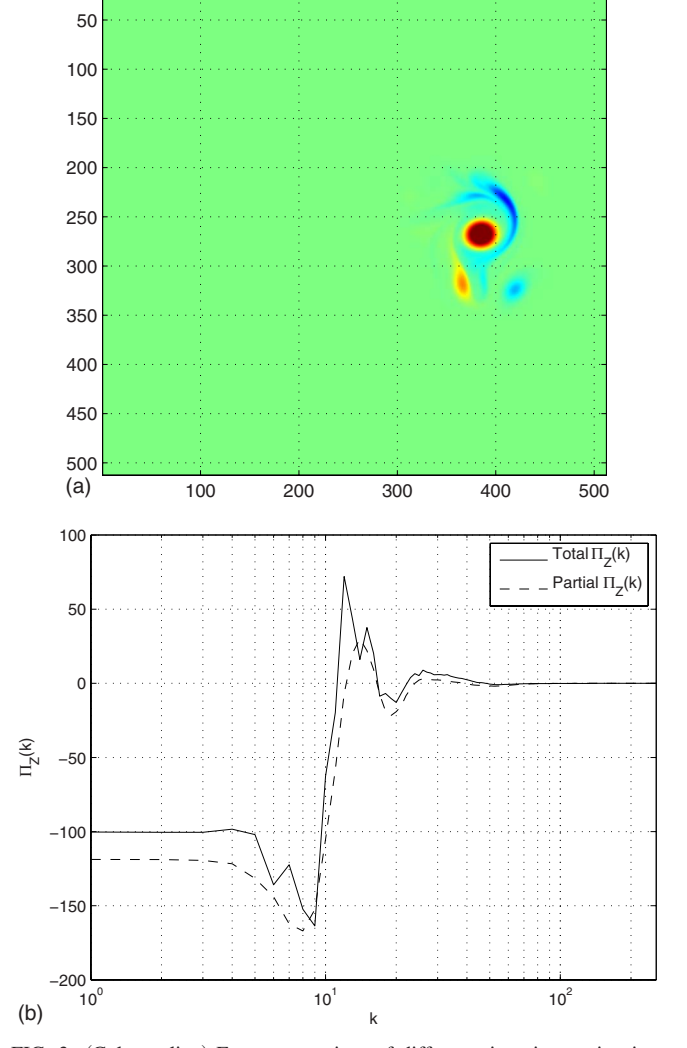


FIG. 3. (Color online) Fourteen vortices of different signs interacting in a  $2\pi$  periodic domain. (a) Partial vorticity field. (b) Enstrophy fluxes for the whole flow and for the selected area.

and an explicit treatment of the convection term. The spatial approximation is performed on uniform staggered grids us-242 ing second-order centered finite differences for the linear 243 terms and a third-order upwind scheme for the convection 244 term. The location of the unknowns enforce the 245 divergence-free equation which is discretized on the pressure 246 points and the choice of uniform grids is necessary to main-247 tain the accuracy of the finite differences schemes. The 248 whole problem is solved by a multigrid method with a cell 249 by cell Gauss–Seidel iterative procedure as smoother. A se-250 quence of grids from  $4 \times 16$  cells up to  $1024 \times 4096$  cells is 251 used on the domain  $\Omega = (0,1) \times (0,4)$  to get accurate results.

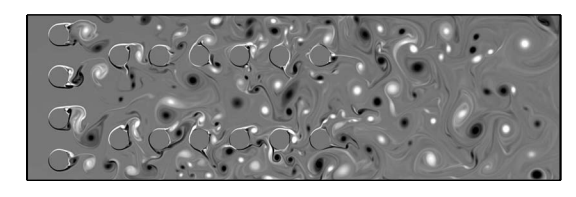


FIG. 4. Snapshot of the vorticity field.

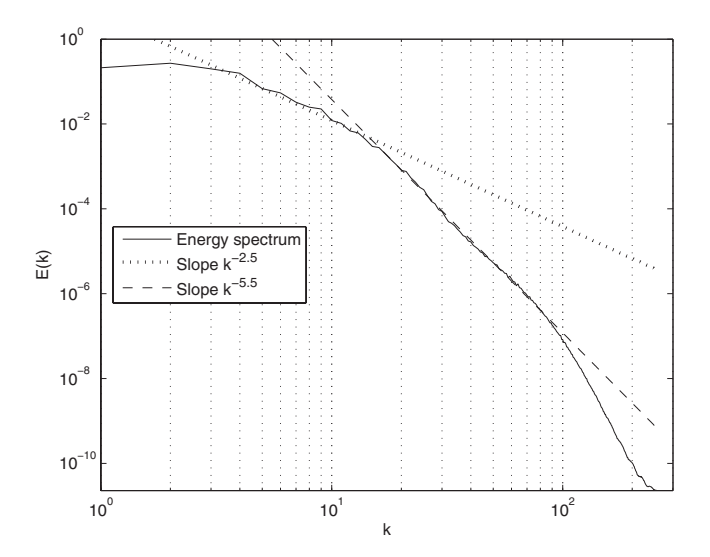


FIG. 5. Energy spectrum.

With respect to the Reynolds number, the finest grid is fine enough to properly capture the whole dynamics.

253

263

Several wavelet bases have been used to test the validity of the interaction function. They all point to the same localizations for the enstrophy transfers, even if the colored patterns were not exactly the same. The method does not depend on the choice of the wavelet basis used in the computations. The results obtained with Daubechies wavelets with ten vanishing moments are presented in here. The wavelet decompositions have been performed over all the scales (ten for this grid).

#### V. NUMERICAL RESULTS

The computation of the enstrophy flux has been per- 264 formed for different configurations (several Reynolds num- 265 bers, several diameters for the obstacles) and many snapshots 266 of the flow for each configuration. We present here the re- 267 sults obtained for a series of 100 images. A snapshot of the 268 vorticity field from the upstream cylinders to the end of the 269 channel is given in Fig. 4. To compute the energy spectrum 270 and the enstrophy flux, we select a square of size L=1 lo-271 cated at the end of the channel as domain of analysis. The 272 cutting process to select this domain creates many disconti- 273 nuities in the velocity and vorticity fields at the boundaries, 274 and thus introduces high frequency Fourier coefficients. This 275 phenomenon is well known from people using the classical 276 fast Fourier transform (FFT) algorithm and has been de- 277 scribed in Refs. 20 and 30. We avoid this problem by using a 278 windowed Fourier transform that removes the spurious coef- 279 ficients created by the discontinuities. We use, for the results 280 presented in this paper, a Tukey window with a parameter 281 equal to 0.1. A larger value for this parameter would cancel a 282 too large amount of the energy and the enstrophy, and a 283 smaller one would not sufficiently smooth the discontinui- 284 ties. The averaged energy spectrum for the 100 first snap- 285 shots is given in Fig. 5. We can observe two slopes on both 286 sides of the injection scale, the first slope being around  $k^{-2.5}$  287 and the second one around  $k^{-5.5}$  and so far from the classical 288 theory that predicts a decrease in  $k^{-3}$ . The first slope is not 289

290 really clear but the second one is evident. Many papers in 291 literature discussed the influence of solid boundaries on the 292 evolution of two-dimensional turbulence in a finite 293 domain. 31–35 According to these studies, the classical theory 294 proposed by Refs. 4 and 5 does not take into account the 295 effects of these particular boundary conditions. Indeed ac-296 cording to Ref. 34, no-slip walls are sources of vorticity fila-297 ments which may affect the behavior of two-dimensional tur-298 bulence. Furthermore, they could show that their influence 299 are not restricted to regions close to the boundary but also 300 extend over the full domain. In our experiments, due to the 301 presence of many cylinders, the flow is dominated by vorti-302 ces created by the cylinders and vorticity filaments in be-303 tween.

The enstrophy flux corresponding to this spectrum is 305 given in Fig. 6. The enstrophy flux is positive above the 306 injection scale, and negative below. The zero crossing corre-307 sponds approximately to the injection scale. Our simulations 308 do not produce a large plateau but an explanation for this is 309 the limitation of range of scales probed and the presence of 310 the boundaries. In our mathematical model, we did not use 311 any artificial dissipation terms which would improve the cre-312 ation of the cascades.

313 The flux presented in Fig. 6 is, in fact, a mean obtained **314** by averaging 100 snapshot fluxes, but does not correspond to 315 the flux of any snapshot. In order to assess the local interac-316 tions in the flow, we have to study the flux of few snapshots **317** separately. We can represent the fluxes of the 100 snapshots 318 in one color representation. The color map goes from blue 319 for negative values to red for positive values. The wavenum-**320** ber range extends from k=1 to k=100 since no flux could be **321** obtained beyond. This representation is given in Fig. 7. We 322 can observe that some snapshots present a strong direct en-323 strophy flux, and others a strong inverse flux leading to the 324 average given in Fig. 6. We can find a very few snapshots 325 with the inverse and direct fluxes in the same time. This 326 proves that the direct enstrophy cascade is not a permanent 327 phenomenon, but rather a transient phenomenon that alter-328 nates with an inverse enstrophy cascade. It can be noticed 329 that these inverse enstrophy flux periods coincide with strong 330 inverse energy flux periods. It is not surprising that strong **331** energy transfers carry also some enstrophy with them. As can 332 be also observed, the inverse energy cascade is only local-**333** ized between k=1 and the injection scale k=8 in accordance 334 with the classical theory.

#### 335 A. Interaction function for the whole field

In order to study the interactions occurring into the en-337 strophy cascade, the interaction function is now computed 338 for few snapshots with strong direct enstrophy fluxes. Snap-339 shots 85 and 92 have been chosen for that purpose. The 340 vorticity field corresponding to snapshot 85 is given in Fig. 341 8(a). Various structures can be observed in this vorticity 342 field. According to previous studies, <sup>19,23</sup> we already know 343 that the vorticity filaments are responsible for the inverse 344 enstrophy cascade, but we do not have yet any information

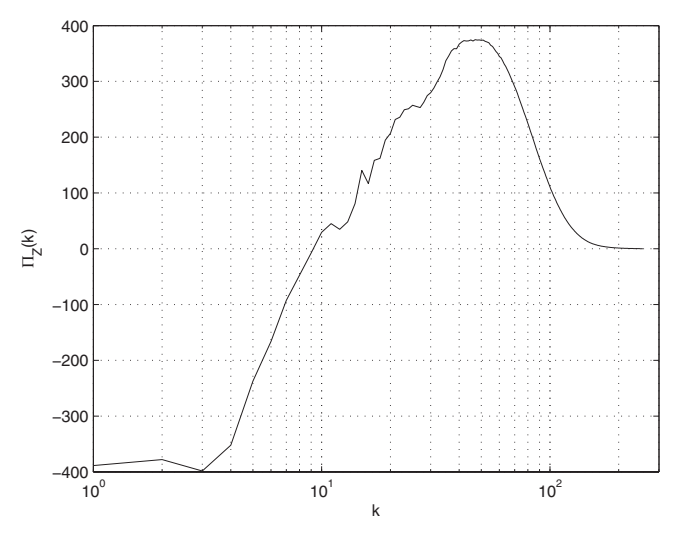
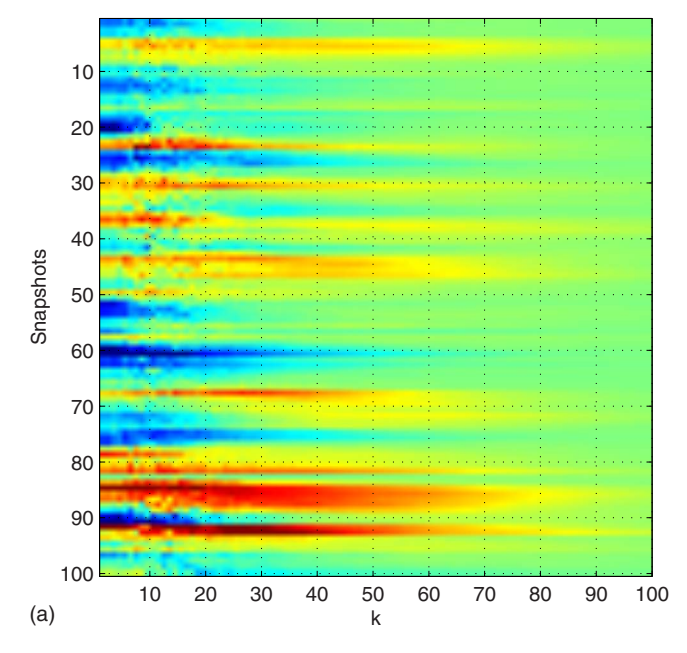


FIG. 6. Enstrophy flux.



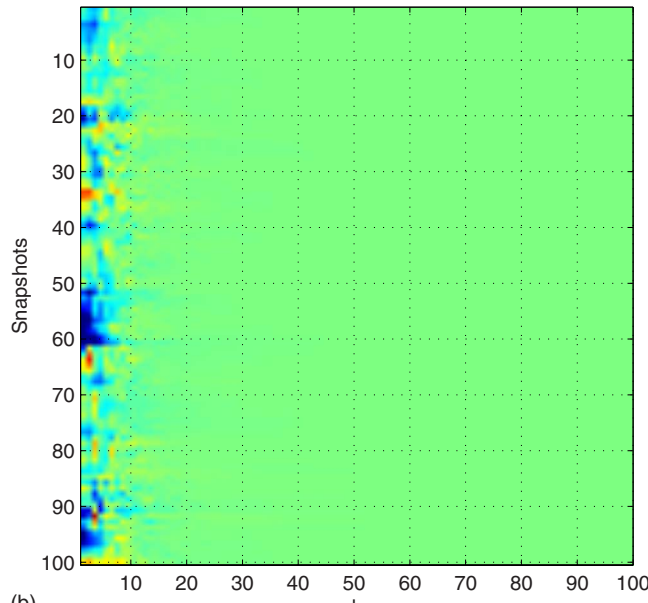


FIG. 7. (Color online) Fluxes for 100 snapshots. (a) Enstrophy flux. (b) Energy flux.

P. Fischer and C.-H. Bruneau Phys. Fluids 21, 1 (2009)

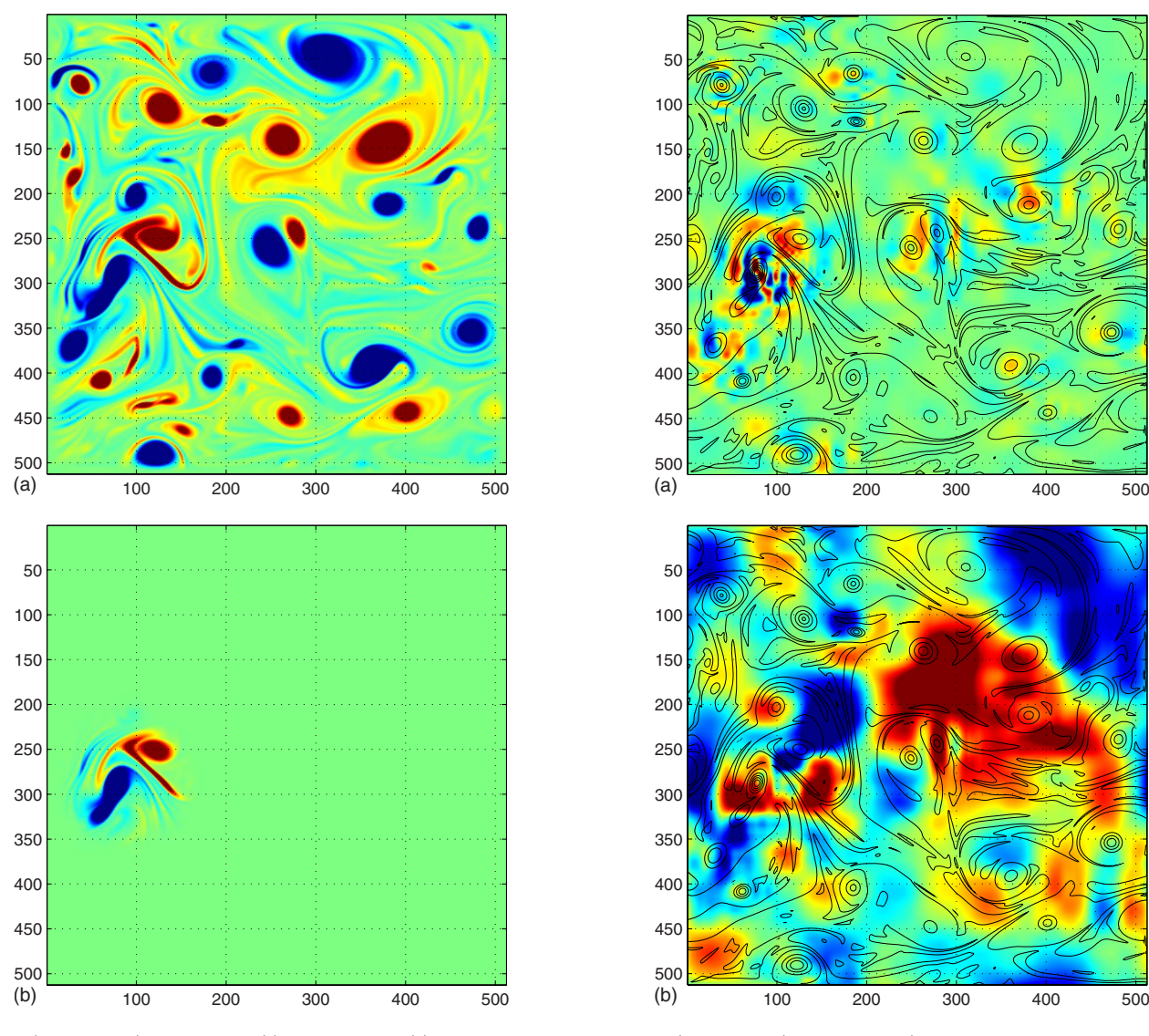


FIG. 8. (Color online) Snapshot 85. (a) Vorticity field. (b) Partial vorticity field.

1-6

FIG. 9. (Color online) Snapshot 85 (vorticity field in contour lines). (a) Enstrophy interaction function. (b) Energy interaction function.

345 about the space localization of the interactions leading to this 346 cascade. The enstrophy interaction function, represented in 347 Fig. 9(a), allows us to get this kind of information. The con-348 trast and the color map have been chosen such that only the 349 most important coefficients are noticeable. Tuning the con-350 trast would make regions appear more colored corresponding 351 to weak enstrophy fluxes. In this snapshot, a region with 352 strong values around (90,285) can be detected. This zone 353 corresponds to interactions between two vortices of opposite 354 signs and where most of the enstrophy cascade occurs. This 355 can be verified by computing the total enstrophy flux and the **356** partial one corresponding to this region. Different strategies 357 can be developed to select this area. We first chose all the 358 points where the enstrophy interaction function is greater 359 than a given threshold (here, the average value between the 360 absolute value maximum and the absolute value mean of the 361 snapshot), and then chose a Gaussian mask that included all 362 these points. The total and partial enstrophy fluxes are given **363** in Fig. 10 and the selected area in the vorticity field in Fig. 364 8(b). As expected, the partial enstrophy flux almost fits the

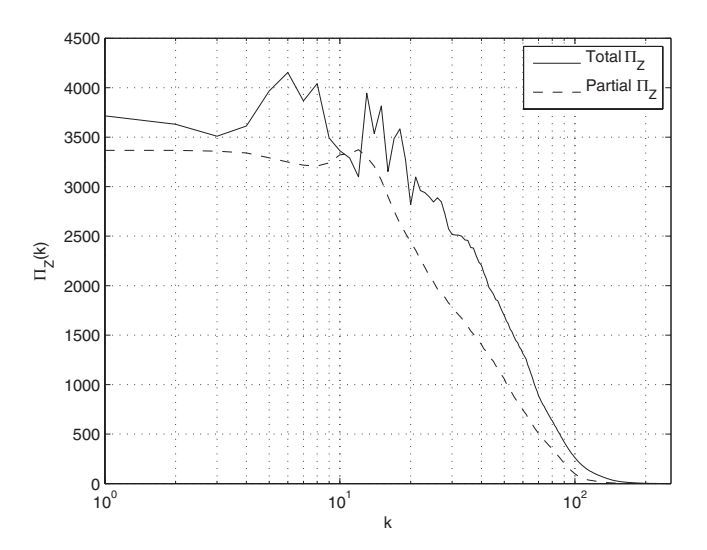


FIG. 10. Enstrophy fluxes (snapshot 85).

400

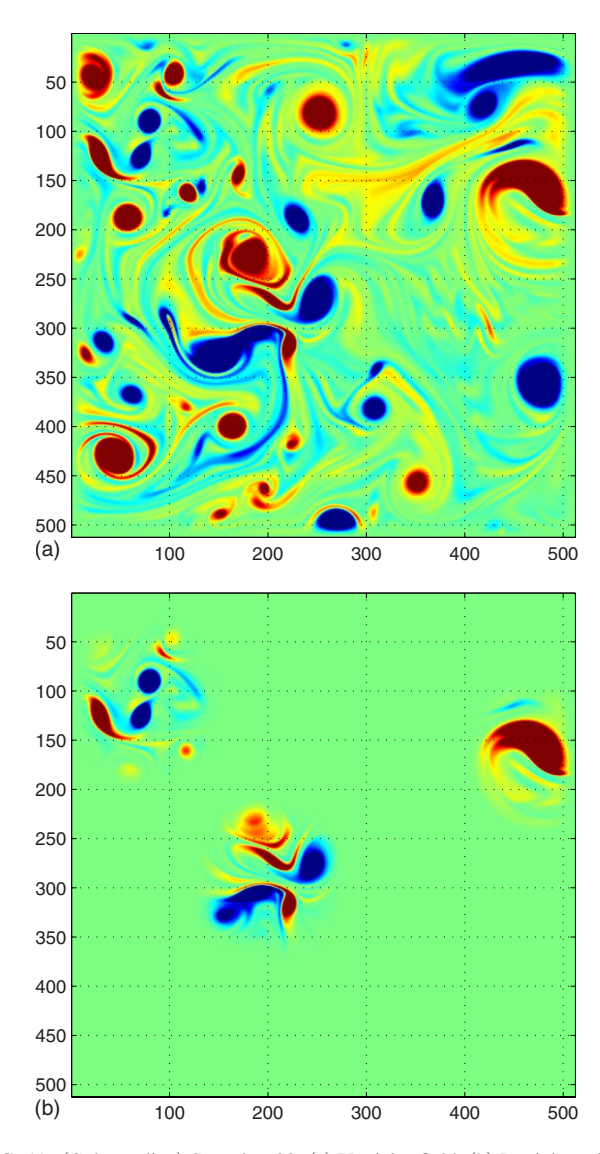


FIG. 11. (Color online) Snapshot 92. (a) Vorticity field. (b) Partial vorticity field.

365 total enstrophy flux proving that the main interactions creat-366 ing the enstrophy cascade effectively take place in this re-367 gion. About 80% of the total enstrophy flux takes place in 368 less than 15% of the flow surface. The energy interaction 369 function, computed in the same way as the enstrophy inter-370 action function, is given in Fig. 9(b). The inverse energy 371 cascade taking place at larger scales, one can observe large 372 regions of interactions for the energy. Consequently, a local 373 analysis of the energy fluxes is not relevant.

A single area of strong interactions has been detected by 375 the interaction function in this snapshot. However, it may 376 happen in some cases that the enstrophy flux is due to inter-377 actions localized in multiple small areas. In this case, the 378 interaction function is still able to precisely locate them as 379 can be verified with the following example. The same kind 380 of analysis is now repeated for snapshot 92 [vorticity field 381 given in Fig. 11(a)]. The corresponding interaction functions 382 are given in Fig. 12.

We can observe that the interactions occur in three dif-384 ferent places. A smaller area around (425,75) can be visually detected in Fig. 12(a) but failed the automatic quantitative selection process. This area could be included in the selected 386 zones group by slightly modifying our threshold. The partial 387 enstrophy flux computed with this fourth zone would be even 388 closer to the total enstrophy flux. The partial and the total 389 vorticity fields are given in Fig. 11. These three areas correspond to places where interactions between different objects 391 occur. We can then compare the total enstrophy flux to the 392 partial one obtained with the three selected regions. The results are given in Fig. 13. For this snapshot too, the enstrophy flux computed in the selected areas almost fits the total 395 enstrophy flux proving that the main interactions creating the 396 enstrophy cascade effectively take place in these three regions. The energy interaction function shows also larger activity area but smaller than those obtained for snapshot 85.

#### B. Interaction function for the filtered fields

Using the same kind of filtering as in Refs. 19, 20, and 401 23, the velocity fields can be cut into two subfields: one 402 subfield with the solid rotation part of the vortices (denoted 403 by the subscript s) and the remaining mainly composed of 404 vorticity filaments that roll up in spiral inside the vortices 405 (denoted by the subscript f). The velocity decomposition v 406 =  $v_s + v_f$  obtained with the wavelet packets based filtering is 407 orthogonal and leads to the energy spectrum decomposition 408

$$E(k) = E_s(k) + E_f(k),$$
 (4) 409

where  $E_s$  is the energy of the solid rotation vortices and  $E_f$  is 410 the energy of the vorticity filaments. Due to this orthogonal 411 decomposition, the enstrophy transfer function can be written as 413

$$T_{Z}(\mathbf{k}) = \widehat{\omega^{*}(\mathbf{k})} \cdot \widehat{(\mathbf{v} \cdot \nabla)\omega(\mathbf{k})}$$

$$= \widehat{\omega^{*}_{s}(\mathbf{k})} \cdot \widehat{(\mathbf{v} \cdot \nabla)\omega_{s}(\mathbf{k})} + \widehat{\omega^{*}_{s}(\mathbf{k})} \cdot \widehat{(\mathbf{v} \cdot \nabla)\omega_{f}(\mathbf{k})}$$

$$+ \widehat{\omega^{*}_{f}(\mathbf{k})} \cdot \widehat{(\mathbf{v} \cdot \nabla)\omega_{s}(\mathbf{k})} + \widehat{\omega^{*}_{f}(\mathbf{k})} \cdot \widehat{(\mathbf{v} \cdot \nabla)\omega_{f}(\mathbf{k})}. \quad (5) \quad 416$$

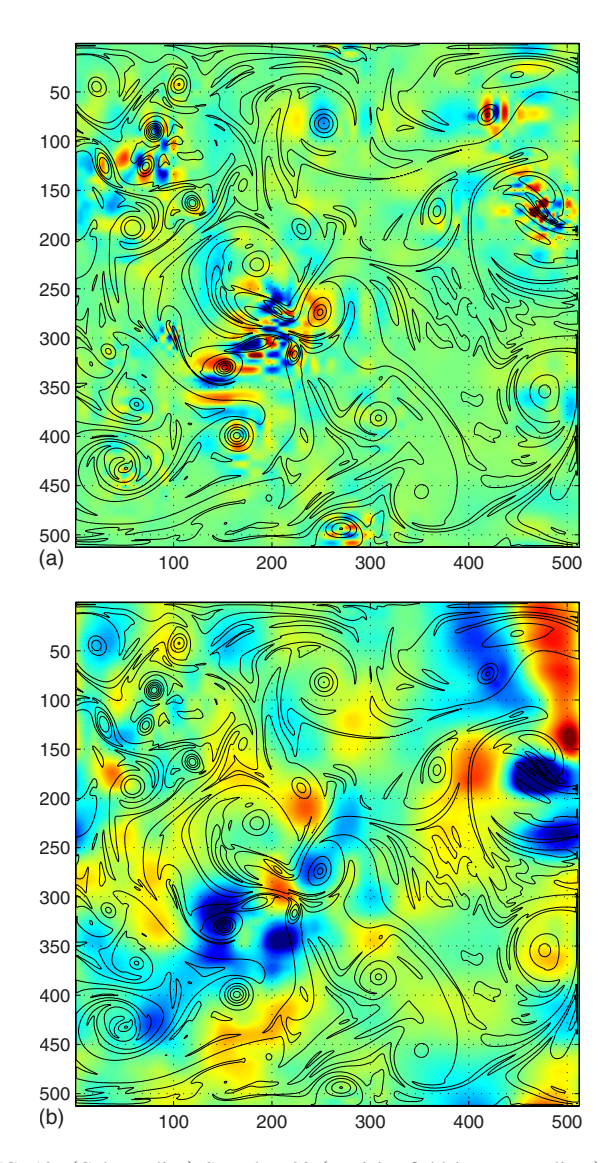
The same decomposition can be also written for the energy transfer function.

417

The global enstrophy transfer is thus split into four parts 419 corresponding to the multiscale transfers from one subfield 420 to itself or to the other one. For instance,  $\widehat{\omega_s}^*(k) \cdot (v \cdot \nabla) \omega_f(k)$  421 is the enstrophy transfer from the vorticity filaments subfield 422 to the solid rotation subfield. The fluxes corresponding to 423 each term in the expression of the total enstrophy transfer 424 function are denoted as, for example,  $\Pi_Z^{f \to s}$  which is the flux 425 corresponding to the transfer term previously described. We 426 already know from previous studies  $^{19,20,23}$  that the filamentary structures are responsible for the enstrophy fluxes. Indeed it has been shown that  $\Pi_Z^{f \to f}$  is the main term in  $\Pi_Z$  429 whereas  $\Pi_E^{s \to s}$  is the main term in  $\Pi_E$ .

Moreover, one can specify how these interactions take 431 place or more exactly what are the media allowing those 432 transfers. Indeed, thanks to the decomposition of the transport operator itself, it has been shown in Ref. 23 that the 434

P. Fischer and C.-H. Bruneau Phys. Fluids 21, 1 (2009)



1-8

FIG. 12. (Color online) Snapshot 92 (vorticity field in contour lines). (a) Enstrophy interaction function. (b) Energy interaction function.

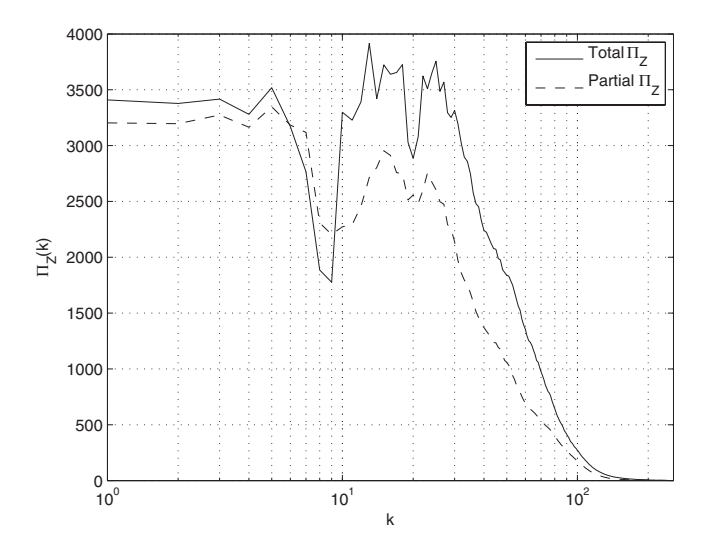


FIG. 13. Enstrophy fluxes (snapshot 92).

solid rotations of the vortices are the means of transport of the energy and enstrophy transfers. Thus the transport opera- 436 tor can be decomposed into two parts: 437

$$(\boldsymbol{v} \cdot \nabla) = (\boldsymbol{v}_s \cdot \nabla) + (\boldsymbol{v}_f \cdot \nabla). \tag{6}$$

By performing this decomposition one can separate the en- 439 strophy transport operated by the solid rotations from the 440 transport operated by the filaments. Finally each term of Eq. 441 (5) can be also split into two parts leading to the following 442 complete decomposition: 443

$$T_{Z}(\mathbf{k}) = \widehat{\omega_{s}^{*}(\mathbf{k})} \cdot \widehat{(\mathbf{v}_{s} \cdot \nabla)} \omega_{s}(\mathbf{k}) + \widehat{\omega_{s}^{*}(\mathbf{k})} \cdot \widehat{(\mathbf{v}_{f} \cdot \nabla)} \omega_{s}(\mathbf{k})$$

$$+ \widehat{\omega_{s}^{*}(\mathbf{k})} \cdot \widehat{(\mathbf{v}_{s} \cdot \nabla)} \omega_{f}(\mathbf{k}) + \widehat{\omega_{s}^{*}(\mathbf{k})} \cdot \widehat{(\mathbf{v}_{f} \cdot \nabla)} \omega_{f}(\mathbf{k})$$

$$+ \widehat{\omega_{f}^{*}(\mathbf{k})} \cdot \widehat{(\mathbf{v}_{s} \cdot \nabla)} \omega_{s}(\mathbf{k}) + \widehat{\omega_{f}^{*}(\mathbf{k})} \cdot \widehat{(\mathbf{v}_{f} \cdot \nabla)} \omega_{s}(\mathbf{k})$$

$$+ \widehat{\omega_{f}^{*}(\mathbf{k})} \cdot \widehat{(\mathbf{v}_{s} \cdot \nabla)} \omega_{f}(\mathbf{k}) + \widehat{\omega_{f}^{*}(\mathbf{k})} \cdot \widehat{(\mathbf{v}_{f} \cdot \nabla)} \omega_{f}(\mathbf{k}) .$$

$$(7) 447$$

The second term in the right hand side of Eq. (7) describes 448 the enstrophy transfer from the solid rotations to themselves 449 by the filamentary structures. The main term responsible for 450 the enstrophy flux, as shown in Ref. 23, can thus be written 451 452

$$\Pi_Z^{f \to f} = \Pi_Z^{f \to s \to f} + \Pi_Z^{f \to f \to f}, \tag{8}$$

where  $\Pi_Z^{f\to s\to f}$  denotes enstrophy transported from filaments 454 to filaments by vortical structures, and  $\Pi_Z^{f\to f\to f}$  is the same 455 but by filamentary structures. The interaction functions cor- 456 responding to the three terms in Eq. (8) are given in Fig. 14, 457 but those corresponding to the other subfields are not given 458 here because they do not present any strong coefficients. One 459 can remark in Fig. 14 that the strong coefficients are local- 460 ized at the same place as in Fig. 9. These figures are coherent 461 with the results obtained in Ref. 23: the filamentary struc- 462 tures are responsible for the enstrophy cascade, and the solid 463 rotations (and not the vorticity filaments since there is no 464 strong coefficients for  $\Pi_Z^{f \to f \to f}$  transport the enstrophy from 465 the filaments to the filaments. The interaction function pro- 466 vides a new insight in the enstrophy cascade since it shows 467 that the enstrophy transfers are not uniformly spread in the 468 whole flow but are localized in particular regions. In all the 469 experiments we performed, enstrophy transfers occur where 470 different sign vortices interact with each other stretching in 471 new filamentary structures.

## C. Attempt of physical interpretations

Many numerical simulations corresponding to different 474 geometries (the same channel but with different numbers of 475 obstacles of various sizes) have been realized and studied. 476 We noticed that some snapshots could present strong direct 477 enstrophy fluxes whereas others present strong inverse en- 478 strophy fluxes. The observations of the corresponding vortic- 479 ity fields could not give any explanation about this two quite 480 different behaviors. However, the wavelet packets filtering 481 leading to the two subfields associated to the interaction 482

472

473

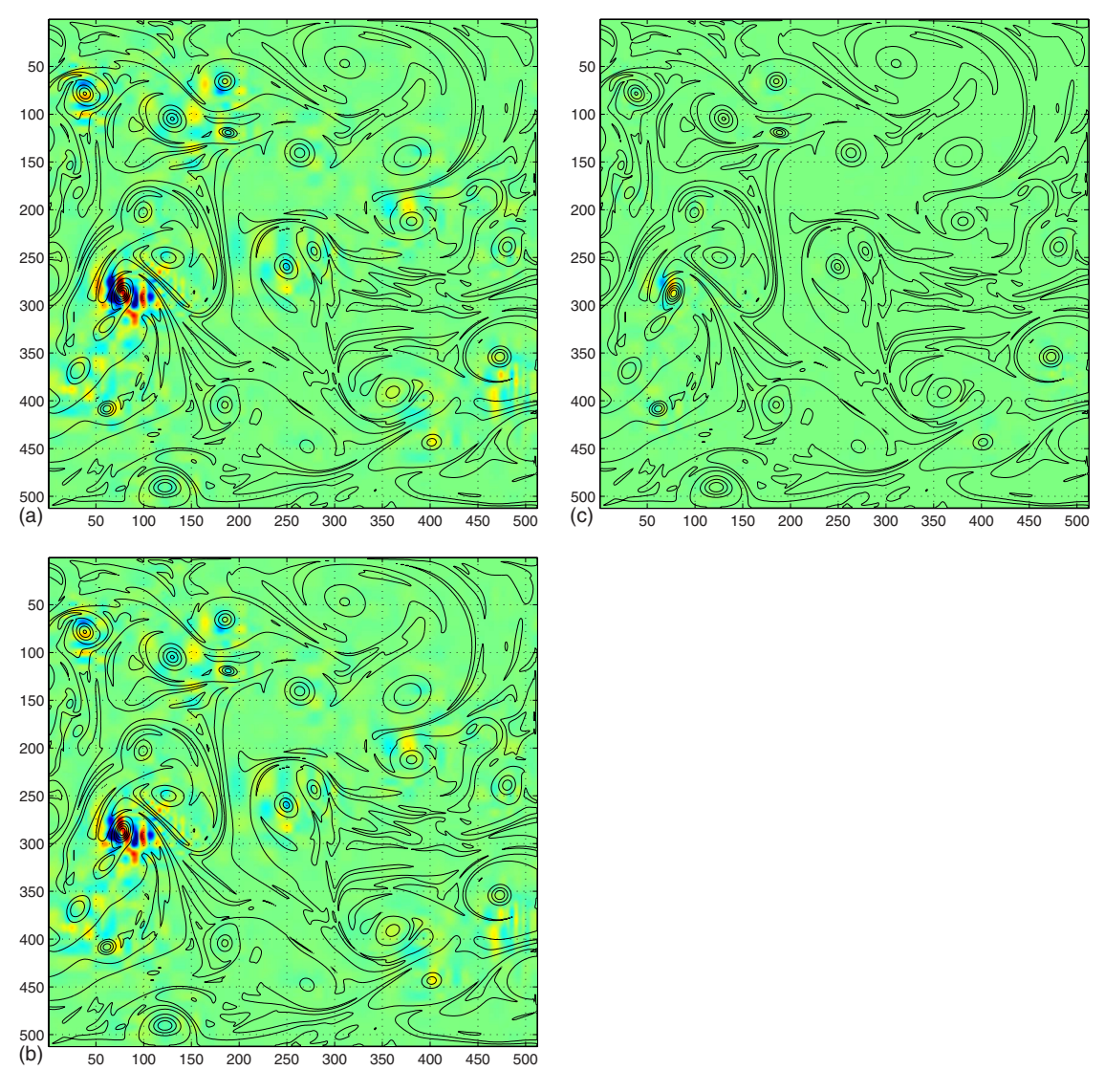


FIG. 14. (Color online) Interaction functions for the filtered fields (snapshot 85). (a)  $\Pi_{Z}^{f-f}$ , (b)  $\Pi_{Z}^{f-s-f}$ , and (c)  $\Pi_{Z}^{f-f-f}$ .

function analysis can give some information about the physi-484 cal process. First, we isolated two of this kind of events from **485** several hundreds available snapshots. They correspond to ex-486 periments on a fine grid with ten small cylinders across the **487** channel and nine small cylinders on each side  $(k_{\text{inj}} \approx 20)$ . The 488 corresponding enstrophy interaction functions are given in **489** Fig. 15. As can be seen on these figures, there is one particu-490 lar zone in each snapshot where the interaction function de-491 tects some strong activities. These zones are located around **492** (170, 180) for snapshot 147 and (200, 100) for snapshot 195. **493** The vorticity fields corresponding to these selected zones are **494** given in Fig. 16. The selected zones correspond to places 495 where vortices of different signs interact with each other. We 496 cannot notice any difference between the two snapshots in 497 Fig. 16 that could explain why they do have completely dif-498 ferent behaviors from an enstrophy flux point of view. In-499 deed, if we study their respective enstrophy fluxes (given in **500** Fig. 17) we can notice that snapshot 147 presents a strong 501 inverse enstrophy cascade whereas snapshot 195 has a strong

direct cascade. In both cases, the selected zones represent less than 15% of the total surface but more than 80% of the 503 enstrophy fluxes.

However, the interaction function for the whole flow 505 does not give any explanation for the difference of enstrophy 506 behaviors between the two snapshots. However we can find a 507 beginning of explanation when studying the interaction functions of the filtered fields obtained through the wavelet packets filtering process. We compute for each snapshot the interaction functions of the eight terms in Eq. (8). For snapshot 511 147, we found that the term  $\Pi_Z^{s \to s \to s}$  is the dominant term whereas for snapshot 195 the term  $\Pi_Z^{f \to s \to f}$  is the main factor 513 in decomposition (8). So in snapshot 195, the enstrophy is 514 transferred from filaments to filaments transported by vortices, leading to the direct enstrophy cascade classical mechanism, whereas in snapshot 147 the enstrophy is transported 517 by vortices from vortices to themselves. A detailed study of 518 the snapshots shows that the mechanism for the direct enstrophy cascade is a strong stretching created by the interactions 520

1-10 P. Fischer and C.-H. Bruneau Phys. Fluids 21, 1 (2009)

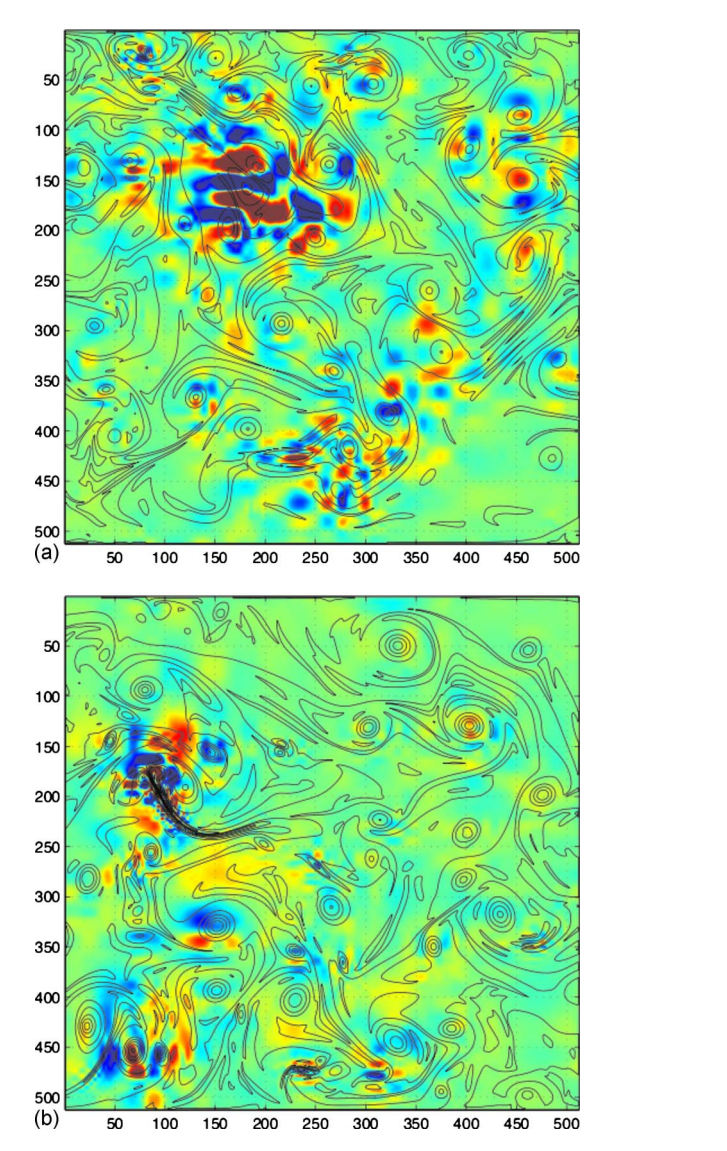


FIG. 15. (Color online) Enstrophy interaction function. (a) Snapshot 147. (b) Snapshot 195.

between two vortices of different signs. This stretching cre-522 ates a long filamentary structure where the transfers are lo-523 cated as it is observed with the corresponding interaction 524 function. We do not see this kind of long filamentary struc-525 ture in snapshot 195, but we can see the interactions between 526 an elongated vortex and another vortex of the same sign. In 527 this case, we can notice that, according to the interaction 528 function, the main interaction takes place between the two 529 like sign vortices.

## 530 VI. CONCLUSION

We propose in this paper an original wavelet-based mathematical tool for studying two-dimensional turbulent flows. This object, called the interaction function, reveals the local enstrophy fluxes in the flow. It is based on the scalar product in a wavelet approximation space of the two terms involved in the computation of the regular enstrophy flux. This study confirms that the enstrophy flux is not a homogeneous phenomenon spread over the whole flow but a local phenomenon corresponding to local interactions. We ob-

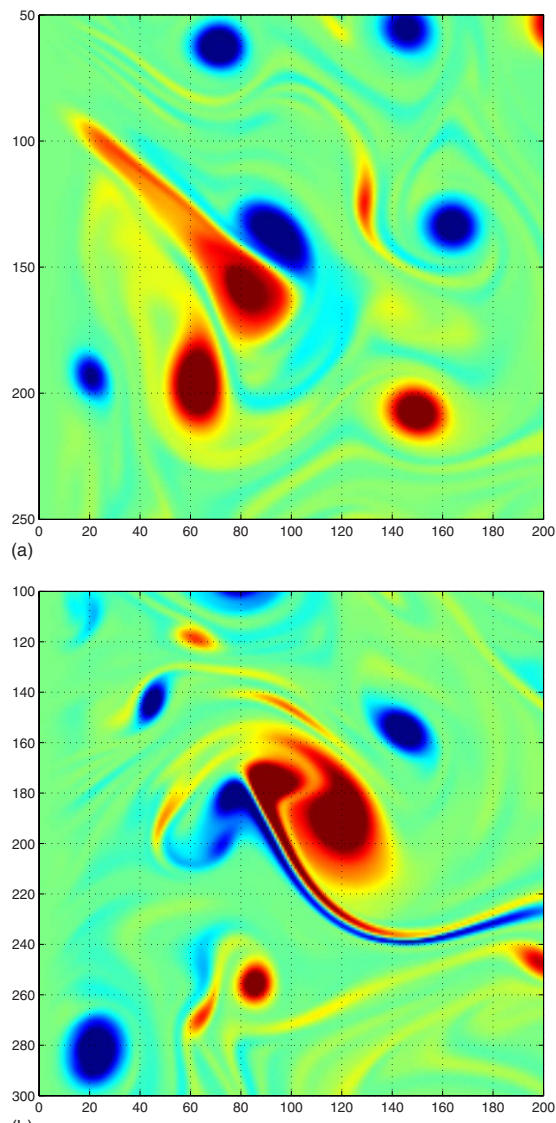


FIG. 16. (Color online) Selected zones of the vorticity fields detected by the interaction function. (a) Snapshot 147. (b) Snapshot 195.

served that in most of the cases more than 80% of the enstrophy flux take place in less than 15% of the flow surface. 541 An important application of the interaction function is ob- 542 tained in association to our regular wavelet packet filtering. 543 Indeed, using these two complementary tools we can observe 544 that inverse enstrophy fluxes are due to interactions between 545 vortices only whereas direct enstrophy fluxes are related to 546 vorticity filaments interactions with vortices. This is mainly a 547 confirmation of what has been thought for a while: the in- 548 verse energy cascade is for a large part due to the merging of 549 vortices and the direct enstrophy cascade is for a large part 550 due to the stretching of vortices that produces very long vor- 551 ticity filaments when they are laminated. In addition, the 552 balance between these two kinds of events governs the level 553 of enstrophy for large scales. When there are more merging 554 events the mean of the enstrophy flux can be negative for 555 scales larger than the injection scale. In the opposite, this 556 mean can be positive when stretching effects dominate in the 557 flow. An important application of our method is related to the 558

583

587

589 590

594

596

597

599

604

606

607

617

620

629

632

633

634

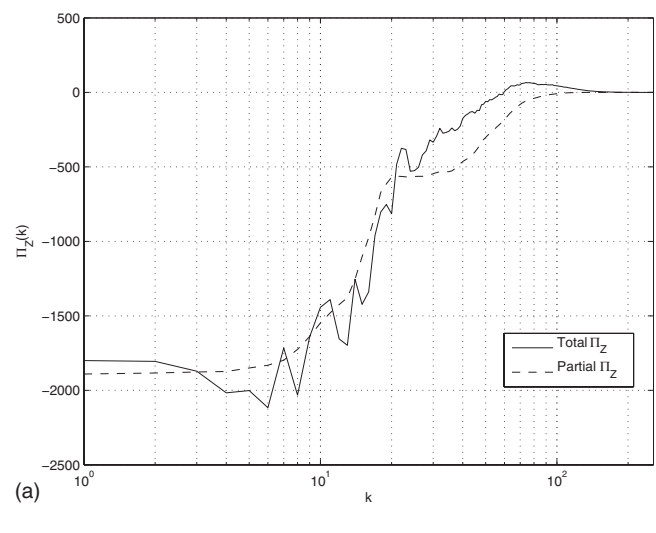
639

641

646

648

651



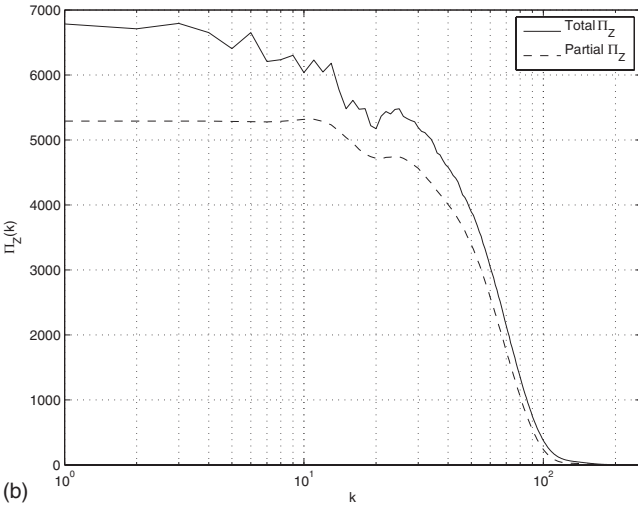


FIG. 17. Enstrophy fluxes for the whole flows and for the selected areas. (a) Snapshot 147. (b) Snapshot 195.

559 study of the walls influence in a turbulent flow. The interac-560 tion function can bring relevant information about the vortic-**561** ity creation by the boundary layers. This is a challenging and 562 open problem that cannot rely on classical tools and that 563 requires efficient and accurate space-scale techniques. An-564 other application is to follow along the time the vortical 565 structures pointed out by the interaction function to deter-566 mine the role of the physical events (merging, stretching, **567** etc.).

#### **568 ACKNOWLEDGMENTS**

The authors thank the referees for their valuable and **570** relevant comments about the manuscript.

- <sup>1</sup>P. Morel and M. Larcheveque, "Relative dispersion of constant-level bal-571 572 loons in 200mb general circulation," J. Atmos. Sci. 31, 2189 (1974).
- <sup>2</sup>E. Lindborg, "Can the atmospheric kinetic energy spectrum be explained 573 574 by two-dimensional turbulence?" J. Fluid Mech. 388, 259 (1999).
- <sup>3</sup>K. K. Tung and W. Orlando, "The k-3 and k-5/3 energy spectrum of 575 atmospheric turbulence: Quasigeostrophic two level model simulation," J. 576 577 Atmos. Sci. 60, 824 (2003).
- R. H. Kraichnan, "Inertial ranges in two-dimensional turbulence," Phys. 578
- Fluids 10, 1417 (1967). 579
- 580 <sup>5</sup>G. K. Batchelor, "Computation of the energy spectrum in homogeneous 581 two-dimensional turbulence," Phys. Fluids 12, II-233 (1969).
  - <sup>6</sup>J. Paret and P. Tabeling, "Experimental observation of the two-

- dimensional inverse energy cascade," Phys. Rev. Lett. 79, 4162 (1997). <sup>7</sup>E. Siggia and H. Aref, "Point-vortex simulation of the inverse energy **584** cascade in two-dimensional turbulence," Phys. Fluids 24, 171 (1981).
- <sup>8</sup>U. Frisch and P. L. Sulem, "Numerical simulation of the inverse cascade in **586** two-dimensional turbulence," Phys. Fluids 27, 1921 (1984).
- <sup>9</sup>L. Smith and V. Yakhot, "Bose condensation and small-scale structure 588 generation in a random force driven two-dimensional turbulence," Phys. Rev. Lett. 71, 352 (1993).
- <sup>10</sup>V. Borue, "Spectral exponents of enstrophy cascade in stationary two-591 dimensional homogeneous turbulence," Phys. Rev. Lett. 71, 3967 (1993). 592
- <sup>11</sup>V. Borue, "Inverse energy cascade in stationary two-dimensional homoge- 593 neous turbulence," Phys. Rev. Lett. 72, 1475 (1994).
- <sup>12</sup>B. Legras, P. Santangelo, and R. Benzi, "High-resolution numerical ex- 595 periments for forced two-dimensional turbulence," Europhys. Lett. 5, 37 (1988)
- <sup>13</sup>H. Kellay, X. L. Wu, and W. I. Goldburg, "Experiments with turbulent **598** soap films," Phys. Rev. Lett. 74, 3975 (1995).
- <sup>14</sup>T. Gotoh, "Energy spectrum in the inertial and dissipation ranges of two-600 dimensional steady turbulence," Phys. Rev. E 57, 2984 (1998). 601
- <sup>15</sup>E. Lindborg, T. M. Alvelius, and P. N. Guzdar, "The kinetic energy spec-602 trum of the two-dimensional enstrophy turbulence cascade," Phys. Fluids 603 **12**, 945 (2000).
- <sup>16</sup>G. Boffetta, A. Celani, S. Musacchio, and M. Vergalossa, "Intermittency 605 in two-dimensional Ekman-Navier-Stokes turbulence," Phys. Rev. E 66, 026304 (2002)
- <sup>17</sup>G. Boffetta, "Energy and enstrophy in the double cascade of two-608 dimensional turbulence," J. Fluid Mech. 589, 253 (2007). 609
- <sup>18</sup>C. H. Bruneau and H. Kellay, "Coexistence of two inertial ranges in two-610 dimensional turbulence," Phys. Rev. E 71, 046305 (2005). 611
- <sup>19</sup>C. H. Bruneau, P. Fischer, and H. Kellay, "The structures responsible for **612** the inverse energy and the forward enstrophy cascades in two-dimensional 613 turbulence," Europhys. Lett. 78, 34002 (2007).
- <sup>20</sup>C. H. Bruneau and P. Fischer, "Influence of the filtering tools on the 615 analysis of two-dimensional turbulent flows," Comput. Fluids 38, 1324 616
- <sup>21</sup>S. Chen, R. E. Ecke, G. L. Eyink, X. Wang, and Z. Xiao, "Physical 618 mechanism of the two-dimensional enstrophy cascade," Phys. Rev. Lett. 619 **91**, 214501 (2003).
- <sup>22</sup>S. Chen, R. E. Ecke, G. L. Eyink, M. Rivera, M. Wan, and Z. Xiao, 621 "Physical Mechanism of the two dimensional inverse energy cascade," Phys. Rev. Lett. 96, 084502 (2006). 623
- <sup>23</sup>P. Fischer, C. H. Bruneau, and H. Kellay, "Multiresolution analysis for 2D **624** turbulence. Part 2: A physical interpretation," Discrete Contin. Dyn. Syst., 625 Ser. B 4, 717 (2007). 626
- <sup>24</sup>M. Farge and G. Rabreau, "Transformee en ondelettes pour detecter et 627 analyser les structures coherentes dans les ecoulements turbulents bidi- 628 mensionnels," C. R. Acad. Sci. de Paris 307, 1479 (1988).
- <sup>25</sup>M. Farge and G. Rabreau, in Scaling, Fractals and Nonlinear Variability 630 in Geophysics, edited by D. Schertzer (Meteorologie Nationale, Paris, 631 1988), pp. 11-16.
- <sup>26</sup>J. Weiss, "The dynamics of enstrophy transfer in two-dimensional hydrodynamics," Physica D 48, 273 (1991).
- <sup>27</sup>H. Kellay and W. I. Goldburg, "Two-dimensional turbulence: a review of 635 some recent experiments," Rep. Prog. Phys. 65, 845 (2002). 636
- <sup>28</sup>P. Angot, C. H. Bruneau, and P. Fabrie, "A penalization method to take 637 into account obstacles in incompressible viscous flow," Numer. Math. 81, 638 497 (1999).
- <sup>29</sup>C. H. Bruneau and M. Saad, "The 2D lid-driven cavity problem revisited," 640 Comput. Fluids 35, 326 (2006).
- <sup>30</sup>C. H. Bruneau and P. Fischer, "Spectra and filtering: A clarification," Int. **642** J. Wavelets, Multiresolut. Inf. Process. 5, 465 (2007). 643
- <sup>31</sup>H. Clercx, "A spectral solver for the Navier-Stokes equations in the 644 velocity-vorticity formulation for flows with two non-periodic directions," 645 J. Comput. Phys. 137, 186 (1997). 647
- <sup>32</sup>H. Clercx and G. van Heijst, "Energy spectra for decaying 2D turbulence in a bounded domain," Phys. Rev. Lett. 85, 306 (2000).
- <sup>33</sup>H. Clercx, A. Nielsen, D. Torres, and E. Coutsias, "Two-dimensional tur-649 bulence in square and circular domains with no-slip walls," Eur. J. Mech. 650 B/Fluids 20, 557 (2001).
- <sup>34</sup>G. Van Heijst, H. Clercx, and D. Molenaar, "The effects of solid bound- 652 aries on confined two-dimensional turbulence," J. Fluid Mech. 554, 411 653 654
- <sup>35</sup>M. Wells, H. Clercx, and G. van Heijst, "Vortices in oscillating spin-up," 655 J. Fluid Mech. 573, 339 (2007).